

## Catalysts Derived from Thermal Treatments of Hydrocalumite-Type Compounds: Synthesis and Application in Transesterification Reactions

Roberta G. Prado,<sup>✉</sup>\*<sup>a,b</sup> Addila G. S. Corrêa,<sup>a</sup> Joyce F. Rodrigues,<sup>a</sup>  
Cristiane A. Scaldaferrri,<sup>b</sup> Fabiana P. de Sousa,<sup>b</sup> Vânia M. D. Pasa,<sup>b</sup>  
Vera R. L. Constantino,<sup>c</sup> Frederico G. Pinto<sup>a</sup> and Jairo Tronto<sup>a</sup>

<sup>a</sup>Laboratório de Compostos Lamelares, Campus de Rio Paranaíba, Universidade Federal de Viçosa, Rodovia MG-230, Km 7, Zona Rural, 38810-000 Rio Paranaíba-MG, Brazil

<sup>b</sup>Laboratório de Ensaios de Combustíveis, Departamento de Química, Universidade Federal de Minas Gerais, Av. Antônio Carlos, 6627, 31270-901 Belo Horizonte-MG, Brazil

<sup>c</sup>Laboratório de Sólidos Lamelares, Departamento de Química Fundamental, Instituto de Química, Universidade de São Paulo, Av. Lineu Prestes, 748, 05508-000 São Paulo-SP, Brazil

Catalyst performance is a relevant factor in biodiesel production because it can affect the efficiency of the process. This work provides a study of the performance of heterogeneous catalysts for biodiesel production derived from thermal-treated hydrocalumite-type compounds. This work aimed to synthesize and characterize hydrocalumite-type compounds intercalated with chloride and nitrate, evaluate the effect of thermal treatments at different temperatures (500, 600, and 750 °C) on these materials, and assess the performance of these materials as catalysts in the transesterification reactions using soybean oil and methanol. The materials were characterized by X-ray diffraction (XRD), vibrational spectroscopy (Fourier transform infrared with attenuated total reflectance (FTIR-ATR)), thermogravimetric analysis coupled to mass spectrometry (TGA-DSC-MS), specific surface area, and X-ray photoelectron spectroscopy (XPS). The results of the transesterification reactions showed that the thermal-treated materials from the hydrocalumite intercalated with chloride presented high catalytic activity, among them, the thermal-treated material at 750 °C presented the highest conversion to methyl esters.

**Keywords:** layered double hydroxides, hydrocalumite, biodiesel, transesterification, heterogeneous catalyst

### Introduction

Biodiesel production technology has been the subject of studies in several countries.<sup>1</sup> These studies aim to reduce dependence and the environmental impact of fossil fuel use. Due to the many advantages of biodiesel, its global consumption increased from 0.25 billion gallons in 2006 to 2.0 billion gallons in 2018.<sup>2</sup>

Biodiesel is a biodegradable fuel produced by transesterification reaction, from renewable sources such as vegetable oils or animal fat. For this reaction, the use of catalysts is highly desirable.<sup>3</sup> Driven by the need to find new catalysts that present high efficiency, lower cost, and apply to environmentally friendly production processes,

several researchers have worked on the development of new heterogeneous catalysts to be applied in transesterification reactions for biodiesel production.<sup>4-7</sup>

Layered double hydroxides (LDH) and their thermal derivatives compounds are commonly used as heterogeneous catalysts in transesterification reactions for biodiesel production.<sup>8,9</sup> Belonging to the LDH family, the hydrocalumite-type compounds have the general formula  $[\text{Ca}_2\text{Al}(\text{OH})_6](\text{A}^{n-})_{(1/n)}\cdot m\text{H}_2\text{O}$ , where  $\text{A}^{n-}$  represents the intercalated anion.<sup>10-13</sup> The hydrocalumite structure consists of the periodic stacking of octahedral layers  $[(\text{Ca}^{2+}, \text{Al}^{3+})(\text{OH})_6]$  of the brucite-type, an  $\text{Mg}(\text{OH})_2$  mineral, where  $\text{Ca}^{2+}$  and  $\text{Al}^{3+}$  cations are distributed in an orderly manner in the positively charged hydroxide layers. In this structure, the  $\text{Al}^{3+}$  cations are hexacoordinated, while the  $\text{Ca}^{2+}$  cations have coordination  $[6 + 1]$ , with the seventh oxygen atom coming from intercalated  $\text{H}_2\text{O}$  molecules. Hydrocalumite

\*e-mail: robertaprado@ufv.br

Editor handled this article: Jaísa Fernandes Soares

has a molar ratio of  $\text{Ca}^{2+}:\text{Al}^{3+}$  equal to 2.<sup>10-14</sup> Different anions can be intercalated in the interlamellar domain of hydrocalumite-type compounds, such as inorganic anions ( $\text{SO}_4^{2-}$ ,  $\text{CO}_3^{2-}$ ,  $\text{NO}_3^-$ ,  $\text{OH}^-$ ,  $\text{Cl}^-$ ), and organic anions (oxalates ( $\text{C}_2\text{O}_4^{2-}$ ), carboxylates, porphyrins, surfactants, polyoxometalates, polymers).<sup>15,16</sup>

Hydrocalumite-type compounds and their thermally composition derivatives have been tested as heterogeneous catalysts in transesterification reactions.<sup>11,17,18</sup> After being heat-treated, hydrocalumite-type compounds lose  $\text{H}_2\text{O}$  and  $\text{CO}_2$ , and decompose to oxides and/or, widely dispersed mixed oxyhydroxides, depending on the treatment conditions applied. When compared to precursor layered materials, these thermal derivatives have greater basicity.<sup>19</sup>

Prado *et al.*<sup>17</sup> synthesized and characterized a mixed oxide of Ca and Al produced by thermal decomposition of a synthetic hydrocalumite. The mixed oxide produced was applied as a heterogeneous catalyst in the transesterification reaction biodiesel production using as reagents refined soybean oil, raw oil from macauba almond, methanol, and ethanol. The catalytic tests indicated that, regardless of the type of oil used, reactions with methanol exhibited more favorable kinetics than those with ethanol. Ethanolysis showed the best result for oil of higher molar mass (soybean) due to the co-solvent effect of ethanol. The catalyst was efficient for transesterification using soybean oil, with conversions above 95% in 1.5 h of reaction under atmospheric pressure and reflux temperature.<sup>17</sup>

Dahdah *et al.*<sup>6</sup> synthesized catalysts from hydrocalumite-type compounds (MgAl-LDH) doped with Ca to be used in transesterification reactions. Calcined (600 °C) and non-calcined materials were tested. In the reaction condition of 6 h, 2.5% of catalyst mass, and a 15:1 methanol:oil ratio, a yield of methyl esters of 95% was achieved.<sup>6</sup>

To the best of our knowledge, other studies reported in the scientific literature about the potential use of thermal-treated hydrocalumite-type compounds as heterogeneous catalysts in transesterification reactions have not presented an in-depth study relating to the different thermal treatments applied to the catalyst with the efficiency of catalysis. Thus, this work aimed at the synthesis and characterization of new heterogeneous catalysts derived from the thermal decomposition of hydrocalumite-type compounds intercalated with chloride and nitrate. These materials were thermally treated at different thermal-treated temperatures and tested as catalysts in transesterification reactions using soybean oil and methanol as reagents.

## Experimental

For the synthesis of hydrocalumite-type compounds

were used:  $\text{CaCl}_2 \cdot 2\text{H}_2\text{O}$  (min. 99%, Dinâmica, São Paulo, Brazil),  $\text{AlCl}_3 \cdot 6\text{H}_2\text{O}$  (min. 99.5%, Dinâmica, São Paulo, Brazil) and  $\text{CaCO}_3$  (min. 99%, Dinâmica, São Paulo, Brazil),  $\text{Ca}(\text{NO}_3)_2 \cdot 4\text{H}_2\text{O}$  (min. 99%, Vetec, Duque de Caxias, Brazil),  $\text{Al}(\text{NO}_3)_3 \cdot 9\text{H}_2\text{O}$  (min. 99%, Sigma-Aldrich, Darmstadt, Germany), NaOH (min. 99%, Isofar, Duque de Caxias, Brazil), and ethanol (min. 92.8%, Tupi, Ibaté, Brazil). All solutions were prepared using ultra-purified water. The gases used for material synthesis and heat treatment were  $\text{N}_2$  (min. 99%) and  $\text{O}_2$  (min. 90%). In the transesterification reactions branded commercial soybean oil and  $\text{CH}_3\text{OH}$  (min. 99.8%, Vetec, Duque de Caxias, Brazil) were used.

The fatty acid profile of the oil was determined by gas chromatography with a flame ionization detector (GC-FID), according to EN14103:2011,<sup>20</sup> involving a hydrolysis step followed by a methylation step under the same conditions described in Bejan *et al.*<sup>21</sup>

### Synthesis of hydrocalumite-type compounds

The synthesis of hydrocalumite-type compounds intercalated with chloride and nitrate anions coded respectively as  $\text{Ca}_2\text{Al\_Cl}$  and  $\text{Ca}_2\text{Al\_NO}_3$ , was carried out by the coprecipitation method at a constant pH value. By this method, the materials were synthesized by coprecipitating cation hydroxides from simple salts.<sup>14,22,23</sup> The synthesis of  $\text{Ca}_2\text{Al\_Cl}$  was performed according to the following procedure: 50 mL of a solution containing the  $\text{CaCl}_2 \cdot 2\text{H}_2\text{O}$  and  $\text{AlCl}_3 \cdot 6\text{H}_2\text{O}$  salts were slowly added (dropwise) over a solution containing 890 mL of decarbonated  $\text{H}_2\text{O}$  and 1600 mL of commercial ethanol. During the synthesis, a solution of NaOH 2.0 mol  $\text{L}^{-1}$  was added to keep the pH value constant at 11.5, for this step an automatic titrator was used. Coprecipitation was carried out at a temperature of 65 °C in a water bath and under mechanical agitation. All synthesis was performed in a closed system under  $\text{N}_2$  atmosphere. For crystallization of the formed material, after the addition of cations, the suspension formed was maintained at a temperature of 65 °C for 24 h. The materials were then washed with decarbonated  $\text{H}_2\text{O}$  and dried using a silica gel desiccator under reduced pressure.

The synthesis of the  $\text{Ca}_2\text{Al\_NO}_3$  was performed in the same way as previously mentioned for the  $\text{Ca}_2\text{Al\_Cl}$ . However, in this case, the reagents used in the cationic solution were  $\text{Ca}(\text{NO}_3)_2 \cdot 4\text{H}_2\text{O}$  and  $\text{Al}(\text{NO}_3)_3 \cdot 9\text{H}_2\text{O}$ .

Studies in literature<sup>24-27</sup> show that LDHs made up of Ca and Al in their composition show catalytic activity when calcined in the range of 600 to 800 °C. Thus, to carry out this work, temperatures of 500, 600, and 750 °C were chosen for the thermal treatment of the synthesized materials. For

the calcination process, a tube furnace was used, under an oxidizing atmosphere with O<sub>2</sub> flow of 150 cm<sup>3</sup> min<sup>-1</sup>, a heating rate of 10 °C min<sup>-1</sup>, and a time interval of 4 h at the threshold temperature.

#### Materials characterization

The analysis of X-ray powder diffraction (XRD) was performed using a Shimadzu (Osaka, Japan) XRD-6000 equipment, with a graphite crystal as monochromator to select the radiation of Cu K $\alpha$  with  $\lambda = 1.54 \text{ \AA}$ , with a step of 0.02° s<sup>-1</sup>. The 2 $\theta$  scan range was 4 to 70°. Molecular absorption spectrophotometry analyses in the infrared region were performed using a Fourier transform spectrophotometer with attenuated total reflectance accessory (FTIR-ATR), Jasco Corporation (Santana de Parnaiba, Brazil), model FTIR 4100. The spectra were obtained with 256 scans, in a wavelength range from 4000 to 400 cm<sup>-1</sup>.

The thermogravimetric analyses coupled with differential exploratory calorimetry and mass spectrometry (TGA-DSC-MS) were obtained using a Netzsch TGA-DSC equipment model STA 409 PC-Luxx, coupled with a Netzsch mass spectrometer model QMS C-Aeolos (Pomerode, Brazil), using alumina crucible. The heating rate was 10 °C min<sup>-1</sup> in O<sub>2</sub> or N<sub>2</sub> atmosphere with 50 cm<sup>3</sup> min<sup>-1</sup> flow, from room temperature up to 1000 °C.

The adsorption/desorption isotherms of N<sub>2</sub> were obtained in an Autosorb iQ2 Quantachrome 2.0 (Graz, Austria) equipment at a liquid nitrogen temperature of 77 K. The samples (100 mg) were degassed at 100 °C for a period of 12 h. Specific areas were measured using the BET method (Brunauer-Emmett-Teller), in the range of 0.05 to 1.00 of relative pressure.

Scanning electron microscopy (SEM) analyses were done using a Quanta 3D FEG scanning microscope (FEI company, Hillsboro, USA). The samples were supported in the sample holder by dispersing the powder on conductive double-sided adhesive tape. A gold coating was applied to the samples before the measurements, using a Sputter BAL-TEC, MED 0.20.

The X-ray photoelectron spectroscopy (XPS) analysis was performed using a UNI-SPECS UHV System commercial spectrometer (Berlin, Germany) with a pressure lower than 5 × 10<sup>-7</sup> Pa. The Al K $\alpha$  line was used (h $\nu$  = 1254.6 eV) as an ionization source and the analyzer pass energy was adjusted to 10 eV. The inelastic noise of the high-resolution spectra C 1s, O 1s, Ca 2p, Cl 2p, Al 2p, and N 1s was subtracted using the Shirley method. The atomic percentage composition of the superficial layer (< 5 nm) was determined by the relative proportions

of the areas of the spectra corrected by Scofield's atomic sensitivity factors, with an accuracy of  $\pm 5\%$ . The spectra were deconvolved using a Voigt function, with Gaussian (70%) and Lorentzian (30%) combinations. The full width at half maximum (FWHM) was between 1.2 and 2.2 eV, and the position of the peaks was determined with an accuracy of  $\pm 0.1$  eV.

#### Catalytic tests

The catalytic tests (transesterification reactions) were performed using branded commercial soybean oil and 3% of catalyst mass in relation to the oil mass. The methanol:oil molar ratio was 14:1. The reaction temperature was reflux, using a heating blanket and 750 rpm magnetic stirring. The total reaction time was 4 h, aliquots were removed every 15 min in the first hour, then an aliquot was removed every hour, with a total of 8 aliquots. The catalyst separation from the transesterification products was carried out by centrifugation and decantation. Then, the products were placed in a water bath for the evaporation of residual methanol.

In the catalyst reuse tests, after the transesterification reaction, the catalyst was recovered by a centrifugation process at 10.000 rpm for 15 min. After this, the separated catalyst was thermally treated at 750 °C for 4 h, under 150 cm<sup>3</sup> min<sup>-1</sup> O<sub>2</sub> flow, and a 10 °C min<sup>-1</sup> heating rate. Then, the resulting material was tested in a new reaction cycle under the same conditions above-mentioned.

The concentration of the methyl esters, obtained in the transesterification reactions, was determined by <sup>1</sup>H nuclear magnetic resonance (NMR), for this, a Bruker Nuclear Magnetic Resonance spectrometer model AVANCE DRX-200 (Rheinstetten, Germany) was used.<sup>28,29</sup>

## Results and Discussion

#### Materials characterization

The diffractograms of Ca<sub>2</sub>Al<sub>2</sub>Cl and their thermal derivatives are shown in Figure 1A. The Ca<sub>2</sub>Al<sub>2</sub>Cl diffractogram (Figure 1Aa) displays an LDH-like profile, with a repetition pattern of the basal peaks (00 $l$ ), with 2 $\theta$  peaks at 11.30 (003), and 22.67 (006). This pattern can be attributed to a hexagonal structure of the material, with a R3 rhombohedral symmetry, in which the anions are intercalated between layers of Ca(OH)<sub>6</sub>·H<sub>2</sub>O and Al(OH)<sub>4</sub>.<sup>12</sup>

After thermal treatment of the material at different temperatures, Figures 1Ab, 1Ac, and 1Ad, the diffractograms indicate the occurrence of the collapse of the layered structure of the pristine material, with the presence of new phases, mainly attributed to the formation of mayenite-type

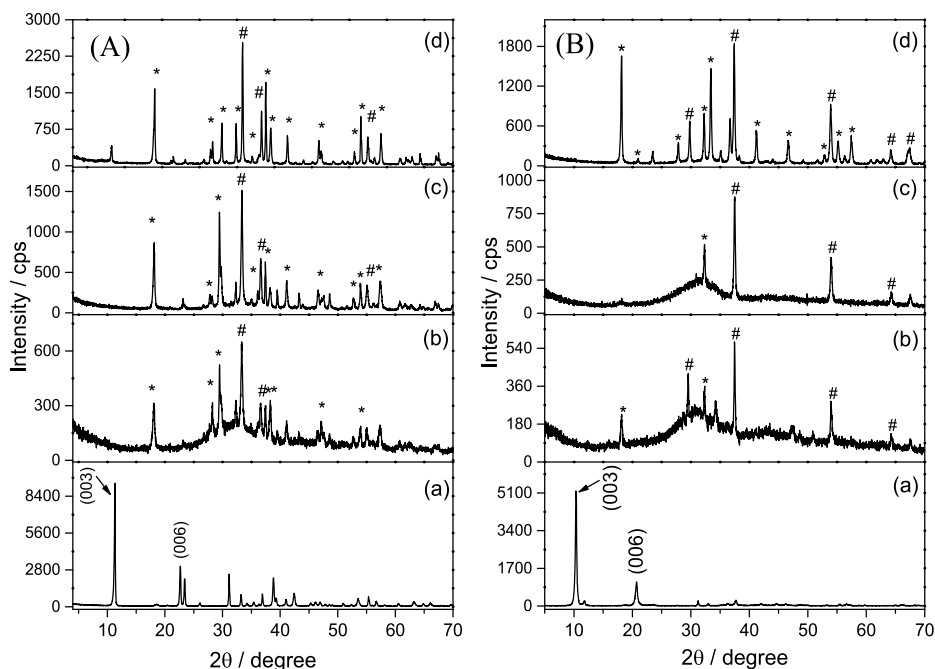


**Figure 1.** (A) Diffractograms for  $\text{Ca}_2\text{Al-Cl}$  (a) pristine (b) 500 °C; (c) 600 °C; and (d) 750 °C. (B) X-ray diffractograms for  $\text{Ca}_2\text{Al-NO}_3$  (a) pristine; (b) 500 °C; (c) 600 °C and (d) 750 °C. \*Mayenite ( $\text{Ca}_{12}\text{Al}_{14}\text{O}_{33}$ ) and \*CaO.

oxide ( $\text{Ca}_{12}\text{Al}_{14}\text{O}_{33}$ ) and calcium oxide (CaO).<sup>30</sup> The results of diffraction analysis for  $\text{Ca}_2\text{Al-NO}_3$  (Figure 1B) were similar to  $\text{Ca}_2\text{Al-Cl}$ , as previously described. Figure 1Ba shows peaks with values of  $2\theta$  in 10.36 (003), and 20.71 (006). For thermally treated materials, Figures 1Bb, 1Bc, and 1Bd, diffractograms indicate that the thermal decomposition of  $\text{Ca}_2\text{Al-NO}_3$  produced materials with phases similar to those found for the thermal decomposition of  $\text{Ca}_2\text{Al-Cl}$ , i.e., mayenite-type oxide ( $\text{Ca}_{12}\text{Al}_{14}\text{O}_{33}$ ) and calcium oxide (CaO).<sup>30</sup> The increase in heat treatment temperature produces more crystalline oxides, as can be observed by the greater intensity of the diffraction peaks related to these phases. Basal spacing values calculated for the synthesized materials are shown in the Supplementary Information section.

Table 1 shows the basal spacing values calculated using the Bragg equation ( $n\lambda = 2d_{hkl}\sin\theta$ , where  $n$  = order of interference (integer),  $\lambda$  = incident wavelength,  $d$  = lattice spacing and  $\theta$  = diffraction angle) for  $\text{Ca}_2\text{Al-Cl}$  and  $\text{Ca}_2\text{Al-NO}_3$ . The basal spacing values found are close to the values reported in the literature for compounds of the hydrocalumite-type, which have been intercalated with the respective anions.<sup>31</sup>

Figure 2A shows the FTIR-ATR spectra for pristine  $\text{Ca}_2\text{Al-Cl}$  and its thermal derivatives. In Figure 2Aa, the band at 796  $\text{cm}^{-1}$  is attributed to the stretching vibration of the Al–O bond, while the band at 512  $\text{cm}^{-1}$  is characteristic of the Ca–O bond.<sup>32,33</sup> The bands at 787 and 519  $\text{cm}^{-1}$  are also related to the metal-oxygen-metal bond (Ca and Al). It

**Table 1.** Basal spacing ( $d$ ) values calculated for the synthesized compounds

Sample	$d / \text{Å}$	$d^a / \text{Å}$
$\text{Ca}_2\text{Al-Cl}$	8.09	7.86
$\text{Ca}_2\text{Al-NO}_3$	8.82	8.79

<sup>a</sup>Literature values.<sup>31</sup>

is observed in the spectra of Figures 2Ab and 2Ac, a band at 780–790  $\text{cm}^{-1}$ , which is attributed to the stretching vibration of the Al–O connection.<sup>33</sup> The bands at 1485–1415  $\text{cm}^{-1}$  are typical of O–C–O stretching vibrations present in  $\text{CO}_3^{2-}$  anions because they are contaminants adsorbed in the materials.<sup>34</sup> The spectrum of Figure 2Ad shows a band at 829  $\text{cm}^{-1}$ , characteristic of C–O stretching, and bands at 675 and 566  $\text{cm}^{-1}$ , referring to the metal-oxygen-metal bond (Ca and Al).<sup>33</sup>

The FTIR-ATR spectra for the pristine  $\text{Ca}_2\text{Al-NO}_3$  and its thermal derivatives are shown in Figure 2B. The bands in the range of 519 to 586  $\text{cm}^{-1}$  present in all materials are characteristic of the Ca–O bond.<sup>32</sup> The bands in regions close to 800  $\text{cm}^{-1}$ , found in the spectra of the thermally treated materials, are attributed to the stretching vibration of the Al–O bond. The bands in the regions close to 1420  $\text{cm}^{-1}$ , found in the spectra in Figures 2Bb, 2Bc, and 2Bd, are typical of anti-symmetric stretching mode  $\text{NO}_3^-$ .<sup>35</sup>

Table 2 shows the BET specific area values for  $\text{Ca}_2\text{Al-Cl}$ ,  $\text{Ca}_2\text{Al-NO}_3$ , and their respective thermal derivatives. The materials have low BET area values. The increase

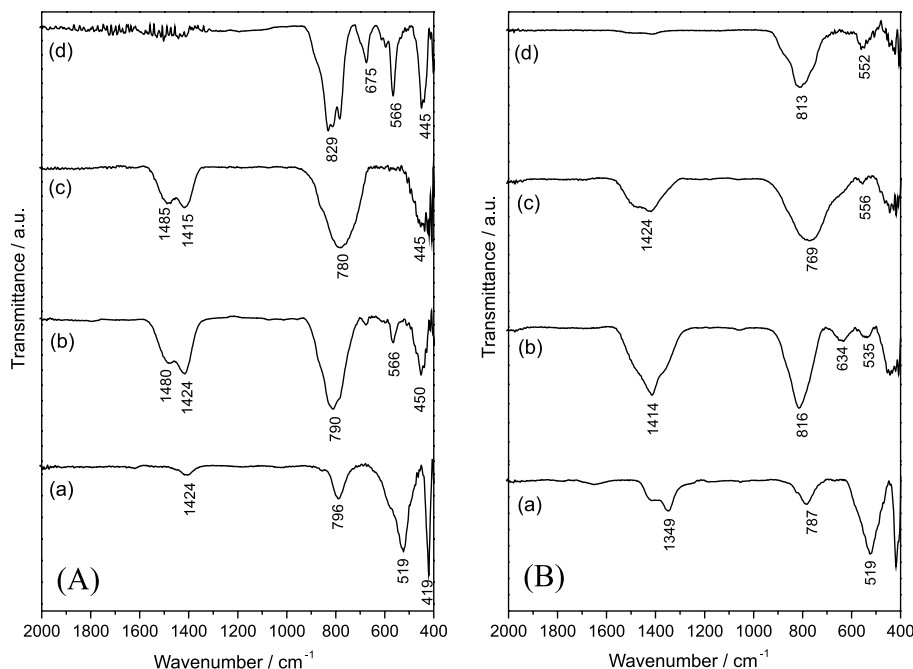


**Figure 2.** (A) FTIR-ATR spectra for  $\text{Ca}_2\text{Al}_2\text{Cl}$  (a) pristine, (b) 500 °C; (c) 600 °C and (d) 750 °C. (B) FTIR-ATR spectra for  $\text{Ca}_2\text{Al}_2\text{NO}_3$  (a) pristine, (b) 500 °C; (c) 600 °C; (d) 750 °C.

in the thermal-treated temperature produced a decrease in the BET area values of the oxides formed. This result corroborates those found in the XRD analysis, in which the increase in heat treatment temperature produced materials with greater crystallinity.

**Table 2.** BET specific area values calculated for synthesized materials

Sample	Specific BET area / ( $\text{m}^2\text{g}^{-1}$ )
$\text{Ca}_2\text{Al}_2\text{Cl}$ 500 °C	10.06
$\text{Ca}_2\text{Al}_2\text{Cl}$ 600 °C	3.49
$\text{Ca}_2\text{Al}_2\text{Cl}$ 750 °C	3.30
$\text{Ca}_2\text{Al}_2\text{NO}_3$ 500 °C	9.76
$\text{Ca}_2\text{Al}_2\text{NO}_3$ 600 °C	9.01
$\text{Ca}_2\text{Al}_2\text{NO}_3$ 750 °C	5.76

BET: Brunauer-Emmett-Teller.

Figure 3 presents the SEM images of  $\text{Ca}_2\text{Al}_2\text{Cl}$  and  $\text{Ca}_2\text{Al}_2\text{NO}_3$ , and their calcined thermal derivatives at 750 °C. The images of  $\text{Ca}_2\text{Al}_2\text{Cl}$  and  $\text{Ca}_2\text{Al}_2\text{NO}_3$ , Figures 3a and 3b, show the presence of some hexagonal platelets, characteristic of LDH particles.

For the  $\text{Ca}_2\text{Al}_2\text{NO}_3$  750 °C, it is possible to notice the presence of very shapeless particles with a size smaller than 10  $\mu\text{m}$ . After the thermal-treated, the  $\text{Ca}_2\text{Al}_2\text{Cl}$  750 °C, Figure 3d, present a compact surface with aggregated plates.

The TGA-DSC-MS curves for  $\text{Ca}_2\text{Al}_2\text{Cl}$  and  $\text{Ca}_2\text{Al}_2\text{NO}_3$  are shown in Figure 4. For  $\text{Ca}_2\text{Al}_2\text{Cl}$ , it is possible to

observe three main thermal decomposition stages, Figure 4a. The first stage occurs from room temperature to approximately 190 °C, with a loss of mass of 14% (DTG peak at 100 °C). In this temperature range, the DSC curve shows an endothermic process, and the MS spectrum detects a fragment  $m/z$  18, attributed to the volatilization of adsorbed  $\text{H}_2\text{O}$  molecules (Figure 4b).

The second stage of thermal decomposition occurs between 190 and 380 °C, and as the DSC curve demonstrates that this stage is an endothermic process. The 15% mass loss is attributed to the volatilization of intercalated water molecules ( $m/z$  18), and the dehydroxylation process of the inorganic layers. The third stage occurs between 500 and 670 °C, with a loss of 2.4% mass. At this stage, the MS spectrum detects the release of a fragment of  $m/z$  44, due to decarbonization, with the release of  $\text{CO}_2$ , Figure 4b. In the DSC curve, the presence of an exothermic event can also be observed at temperatures above 780 °C. At this stage, the loss of mass is approximately 1.13%.<sup>14</sup>

The  $\text{Ca}_2\text{Al}_2\text{NO}_3$  thermogram has four main thermal decomposition steps, all of which are endothermic, Figure 4c. The first stage occurs from room temperature to 200 °C, with a loss of 14% mass. The MS spectrum detects a fragment of  $m/z$  18, Figure 4d, corresponding to the dehydration of the material. The second stage of decomposition occurs between 200 and 400 °C, with a loss of 16% mass. In this temperature region, the MS spectrum detects a fragment  $m/z$  18, related to the loss of

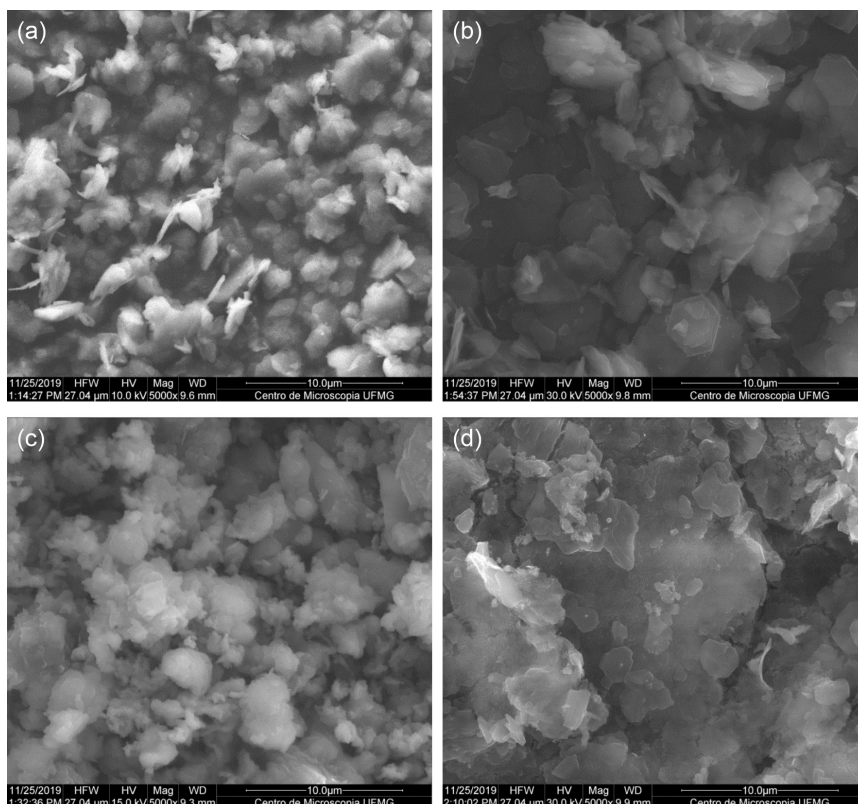


**Figure 3.** SEM images of (a)  $\text{Ca}_2\text{Al}_2\text{Cl}$ , (b)  $\text{Ca}_2\text{Al}_2\text{NO}_3$ , (c)  $\text{Ca}_2\text{Al}_2\text{Cl}$  750 °C, and (d)  $\text{Ca}_2\text{Al}_2\text{NO}_3$  750 °C.

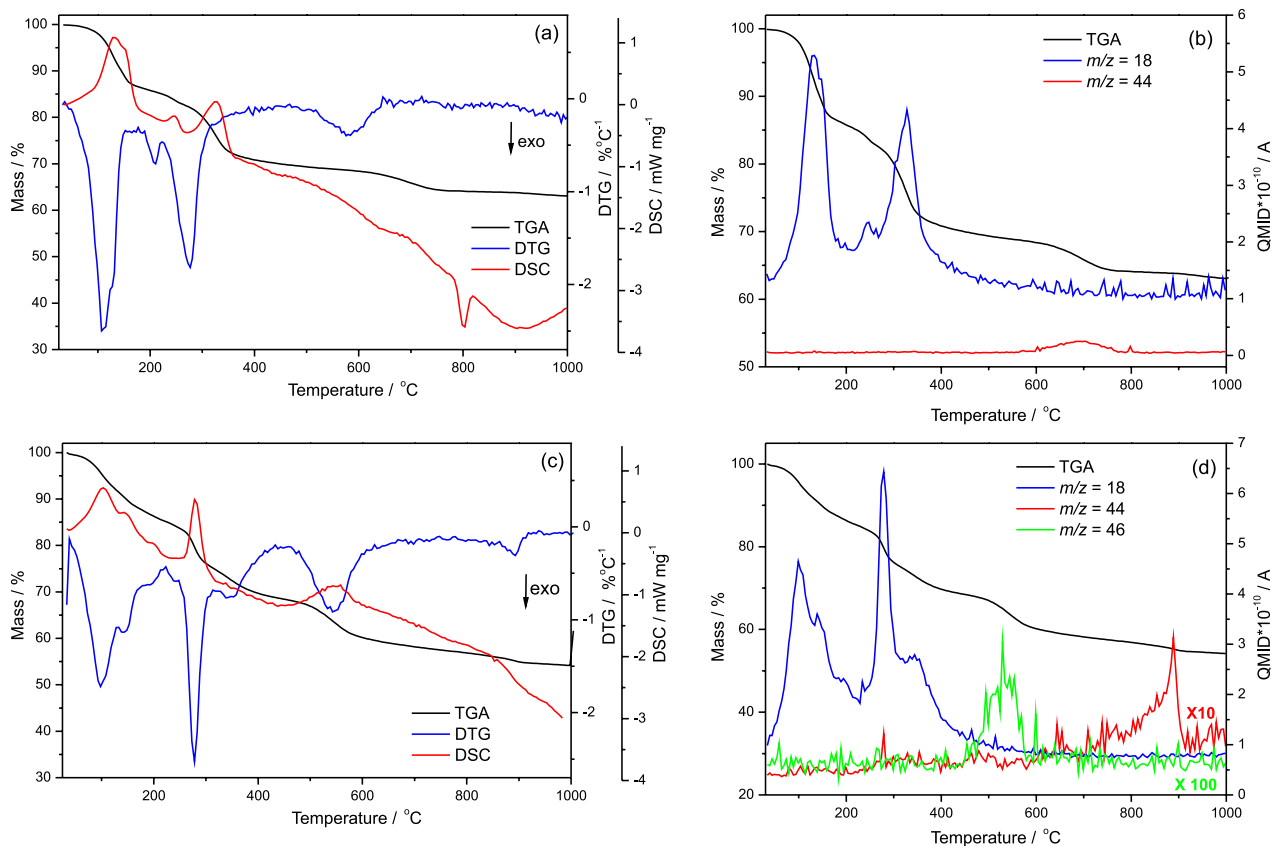


**Figure 4.** (a) TG-DTG-DSC and (b) TG-MS analysis for  $\text{Ca}_2\text{Al}_2\text{Cl}$ , (c) TG-DTG-DSC and (d) TG-MS analysis for  $\text{Ca}_2\text{Al}_2\text{NO}_3$ . The  $m/z$  44 and 46 signs were multiplied by 10 and 100 times, respectively.

interlamellar H<sub>2</sub>O, and the dehydroxylation layers process. The third stage occurs between 400 and 660 °C, with a loss of 11% mass. In this temperature region, the MS spectrum detects the presence of the fragment (*m/z* 46), related to the loss of NO<sub>2</sub>. The fourth stage of thermal decomposition occurs between temperatures of 800 and 950 °C, with a loss of 2.4% mass. In this stage, the MS spectrum detects a fragment with *m/z* 44, related to the loss of CO<sub>2</sub>.<sup>19</sup>

TG-DSC-MS analysis corroborates with FTIR-ATR spectra indicating the presence of CO<sub>2</sub> contaminant in both pristine materials. It is important to note that in the decomposition of Ca<sub>2</sub>Al(NO<sub>3</sub>)<sub>3</sub>, the elimination of NO<sub>2</sub> occurs from 400 °C. On the other hand, Ca<sub>2</sub>AlCl will only release chlorine, as a HCl fragment, at temperatures above 850 °C, indicating that even after thermal-treated, these materials still have Cl in their structures.<sup>36</sup> The presence of Cl in calcined materials was also detected in XPS analysis, as will be discussed later. This result points out an interesting differential regarding these materials, showing a relevant contribution in terms of the synthesis of new basic heterogeneous catalysts.

The surface atomic composition of materials calcined at 750 °C, determined by XPS analysis, is shown in Table 3. The Ca/Al ratio measured in the materials was 1.36 and 1.23 for Ca<sub>2</sub>AlCl 750 °C, and Ca<sub>2</sub>Al(NO<sub>3</sub>)<sub>3</sub> 750 °C, respectively. For Ca<sub>2</sub>AlCl 750 °C, there is 6.3% of Cl present in the sample. Prado *et al.*<sup>17</sup> also observed by TG-MS and energy-dispersive X-ray spectroscopy (EDS) analyses, that Cl present in hydrocalumite-type compounds remains in the material after thermal-treated at 750 °C.

**Table 3.** Composition of samples Ca<sub>2</sub>AlCl 750 °C and Ca<sub>2</sub>Al(NO<sub>3</sub>)<sub>3</sub> 750 °C

Element	Atomic <sup>a</sup> / %	
	Ca <sub>2</sub> AlCl 750 °C	Ca <sub>2</sub> Al(NO <sub>3</sub> ) <sub>3</sub> 750 °C
Carbon (C 1s)	37	33
Oxygen (O 1s)	34	44
Calcium (Ca 2p)	13	13
Aluminum (Al 2p)	10	11
Nitrogen (N 1s)	–	< 0.1
Chlorine (Cl 2p)	6.3	0.1

<sup>a</sup>Error: ± 5%.

The carbon present in the samples (C–H, C–O, C=O, and O–C=O) comes from the CO<sub>3</sub><sup>2-</sup>, originating from the CO<sub>2</sub> in the medium.<sup>37</sup> Moreover, in the case of Ca<sub>2</sub>AlCl it was possible to confirm the presence of chlorine in the calcined material, which is the main difference between the composition of the two heat-treated materials.

XPS spectra are presented in Figure 5a (Ca 2p) and Figure 5b (Al 2p) of the Ca<sub>2</sub>AlCl 750 °C and Figure 5c

(Ca 2p) and Figure 5d (Al 2p) of the Ca<sub>2</sub>Al(NO<sub>3</sub>)<sub>3</sub> 750 °C samples.

It is possible to evaluate the ratio of oxides (CaO, Al<sub>2</sub>O<sub>3</sub>) and oxyhydroxide (Ca<sub>2</sub>Al(OH)<sub>7</sub>) on the surface of the catalysts. The percentages of the compounds and the full width at half maximum (FWHM) of Ca<sub>2</sub>Al(OH)<sub>7</sub>, CaO, and Al<sub>2</sub>O<sub>3</sub> are presented in Table 4. The presence of these compounds is important because they have demonstrated catalytic activity in transesterification reactions with vegetable oil.<sup>38,39</sup> The Ca<sub>2</sub>AlCl 750 °C showed a higher percentage of superficial CaO, 39.7%, when compared to the Ca<sub>2</sub>Al(NO<sub>3</sub>)<sub>3</sub> 750 °C, 29.8% (sum of areas CaO 2p), which may be related to the higher catalytic activity of this material in the catalytic tests.

### Catalytic tests

The conversion curves of the percentage the methyl esters *versus* time, for the transesterification reactions, using the Ca<sub>2</sub>AlCl and Ca<sub>2</sub>Al(NO<sub>3</sub>)<sub>3</sub> thermal derivatives catalysts, are shown in Figures 6a and 6b, respectively.

The Ca<sub>2</sub>AlCl 750 °C catalyst showed 99% of methyl esters conversion after 2 h of reaction. When this catalyst was heat-treated at 600 °C, 81% methyl esters were converted after 4 h of reaction. When Ca<sub>2</sub>Al(NO<sub>3</sub>)<sub>3</sub> was treated at high thermal-treated temperatures, it also presented higher conversion rates of methyl esters in the catalytic tests. A conversion of 91% was achieved after 3 h of reaction of the material calcined at 750 °C, and when the catalyst was thermal-treated at 600 °C, the conversion decreased to 70%. Both catalysts exhibited low catalytic activity when calcined at 500 °C.

When comparing the heat-treated materials, Ca<sub>2</sub>AlCl 750 °C showed better catalytic results, that is, greater conversions of soybean oil into methyl esters in shorter reaction times. Results reported in the scientific literature show that the Mg/Al content in the catalysts is directly related to the basicity of the materials, which is one of the main factors of catalytic activity in the transesterification reaction.<sup>40</sup> According to Cavani *et al.*<sup>31</sup> the number of basic sites increased with the Mg/Al ratio, therefore, when increasing the aluminum content in a mixed oxide (a thermal derivative LDH), the density of basic sites decreases.<sup>40</sup> The Ca<sub>2</sub>Al(NO<sub>3</sub>)<sub>3</sub> 750 °C showed lower catalytic activity and a higher content of Al<sub>2</sub>O<sub>3</sub>, when compared to Ca<sub>2</sub>AlCl 750 °C, 49 and 37%, respectively (Table 4).

The difference in composition between Ca<sub>2</sub>AlCl 750 °C and Ca<sub>2</sub>Al(NO<sub>3</sub>)<sub>3</sub> 750 °C is due to the intercalated anion, in the case of chloride, it remains after heat treatment, and nitrate is not found in the catalyst after

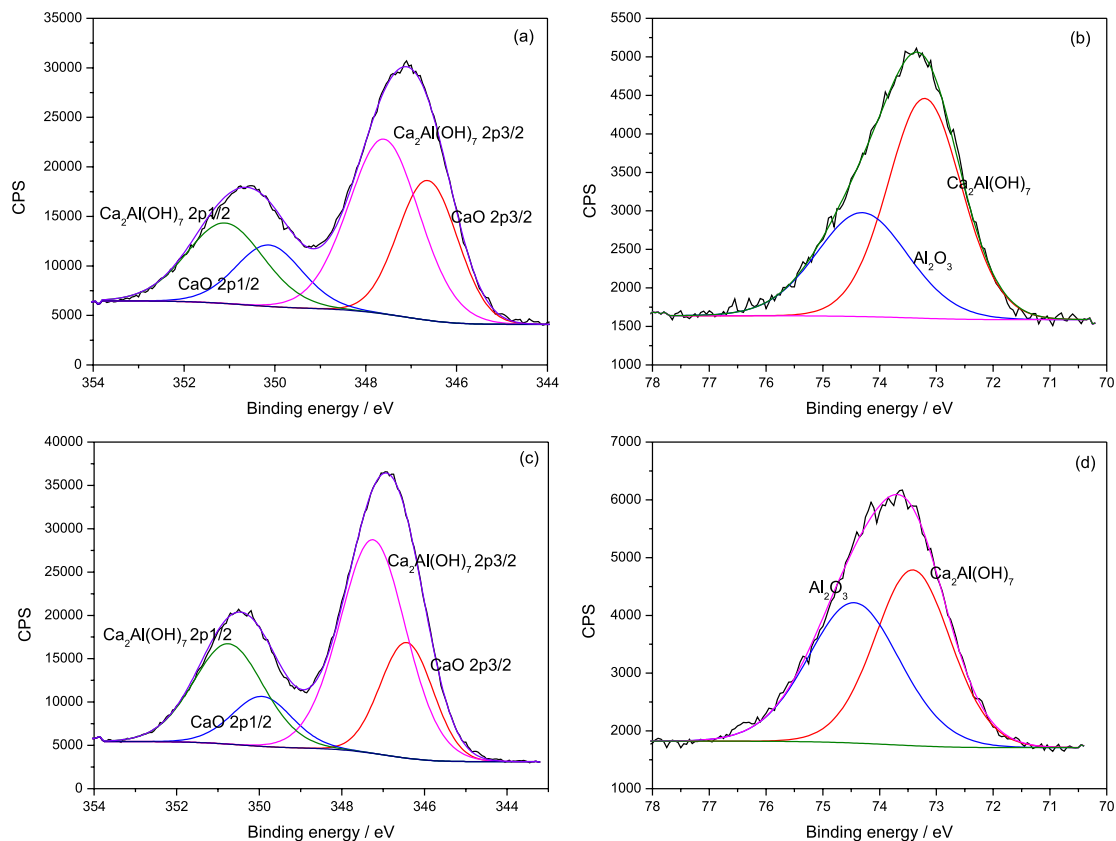


**Figure 5.** XPS spectra for (a) Ca 2p and (b) Al 2p of the  $\text{Ca}_2\text{Al-Cl}$  750 °C and (c) Ca 2p and (d) Al 2p of the  $\text{Ca}_2\text{Al-NO}_3$  750 °C samples.

**Table 4.** Composition and full width at half maximum (FWHM) of  $\text{Ca}_{2p}$  and  $\text{Al}_{2p}$  from XPS spectra

Signal attribution (E / eV)	$\text{Ca}_2\text{Al-Cl}$ 750 °C		$\text{Ca}_2\text{Al-NO}_3$ 750 °C	
	FWHM	Area / %	FWHM	Area / %
$\text{Ca}_{2p}$	CaO 2p3/2 (346.63)	1.543	26.45	19.88
	CaO 2p1/2 (350.13)	1.724	13.25	9.96
	$\text{Ca}_2\text{Al(OH)}_7$ 2p3/2 (347.60)	1.841	40.18	46.75
	$\text{Ca}_2\text{Al(OH)}_7$ 2p1/2 (351.10)	2.000	20.12	23.41
$\text{Al}_{2p}$	$\text{Ca}_2\text{Al(OH)}_7$ (73.21)	1.531	63.04	50.93
	$\text{Al}_2\text{O}_3$ (74.31)	1.900	36.96	49.07

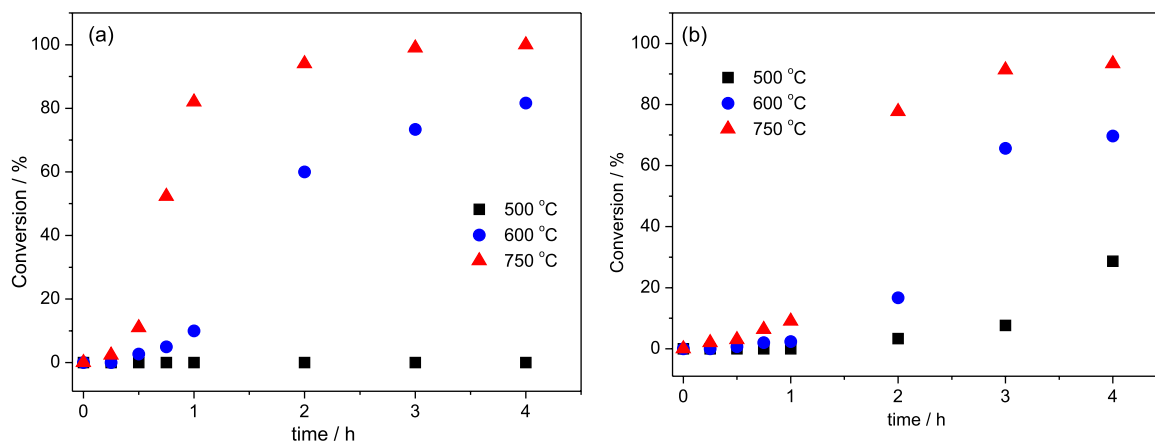


**Figure 6.** Variation of the conversion as a function of time for the transesterification reaction using (a)  $\text{Ca}_2\text{Al-Cl}$  and (b)  $\text{Ca}_2\text{Al-NO}_3$ , calcined at different temperatures.

heat treatment (Table 3). This result shows that the type of intercalated anion between the hydrocalumite layers gives rise to different types of thermal-treated materials which consequently affects the catalytic activity of these materials.

The low specific area values found in the catalysts (Table 2) could limit the diffusion of the reactants to their available basic sites. Consequently, they could have presented a lower catalytic power when compared to catalysts with high surface areas.<sup>41</sup> Despite this, the catalysts synthesized in this work showed high conversion rates to methyl esters when compared to other catalysts reported in the scientific literature.<sup>6,42</sup> The catalytic result presented is possibly due to the synergy between two or more active components present in the catalysts, such as the simple and mixed oxides.<sup>43,44</sup>

Figure 7 shows the results of the catalyst reuse tests carried out with the catalysts thermal-treated at 750 °C. In the second reaction cycle, there was a lower conversion for both catalysts, 53% for Ca<sub>2</sub>Al-Cl and 12% for Ca<sub>2</sub>Al-NO<sub>3</sub>. In the third cycle, the Ca<sub>2</sub>Al-Cl obtained a conversion of 12% while there was no measurable conversion value for Ca<sub>2</sub>Al-NO<sub>3</sub>.

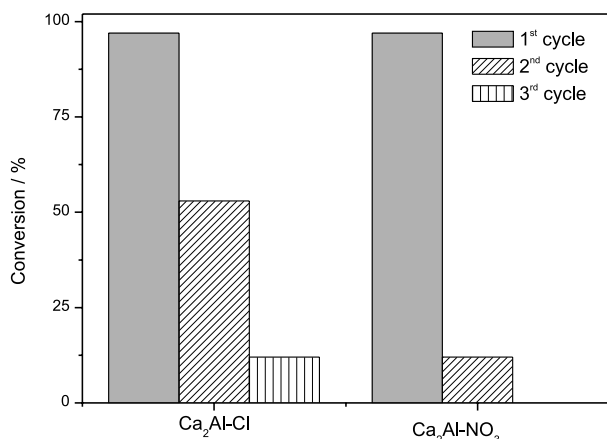


**Figure 7.** Catalyst reuse cycles of Ca<sub>2</sub>Al-Cl and Ca<sub>2</sub>Al-NO<sub>3</sub> thermal-treated at 750 °C.

The catalytic activities of the materials were reduced at each cycle until the complete deactivation of the catalysts. One proposal for what might have happened is that the metal oxides were “poisoned” by absorption of H<sub>2</sub>O, CO<sub>2</sub>, and/or by the reaction medium (e.g., methyl ester, glycerol, oil). In this case, washing the materials after each cycle, before the calcination process, can contribute to a better performance of the catalysts in the reuse cycles.<sup>45</sup> Another possibility that could explain the catalytic deactivation observed for reused samples is some structural modification presented in the materials after the catalytic reactions.<sup>40</sup>

## Conclusions

The thermal treatment of the hydrocalumite-type materials produced a mixture of mayenite-type compound and calcium oxide, as shown in the results of XRD and FTIR-ATR analysis. The results of the TG-MS-DSC showed that the nitrate intercalated in the LDH is released at a temperature range of 400 and 660 °C. However, when LDH is intercalated with chloride, the intercalated anion is not released at the temperatures tested in this work, only being present in the catalyst after thermal-treated at 750 °C, as shown in the XPS analysis. The XPS analysis revealed that the main differences in the surface composition of the Ca<sub>2</sub>Al-Cl 750 °C and Ca<sub>2</sub>Al-NO<sub>3</sub> 750 °C catalysts, in addition to the presence of chloride in the first one, is the oxide/oxyhydroxide ratio.

Among the thermal-treated temperatures tested (500, 600, and 750 °C), 750 °C was the one that generated the most active catalysts in the transesterification reaction of soybean oil with methanol. For both catalysts calcined at 750 °C, the conversion to methyl esters was greater than 90%, with 2 h of reaction for Ca<sub>2</sub>Al-Cl 750 °C and 3 h for Ca<sub>2</sub>Al-NO<sub>3</sub> 750 °C. Thus, the intercalated anion influenced the catalytic activity, the thermal-treated material derivative from the hydrocalumite type-material intercalated with chloride showed better results when compared with the one intercalated with nitrate.

## Supplementary Information

In the supplementary material, the characterization of soybean oil is presented. Supplementary data are available free of charge at <http://jbc.ssbq.org.br> as PDF file.

## Acknowledgments

We thank Dr Peter Hammer from the Universidade Estadual Paulista (UNESP), Laboratório de Espectroscopia de Fotoelétrons - LEFE (Photoelectron Spectroscopy Laboratory) for XPS analysis. We also thank the Rede Mineira de Química (RQ-MG) and, the Programa de Pós-Graduação Multicêntrico em Química de Minas Gerais (PPGMQ-MG), Fundação de Amparo à Pesquisa do Estado de Minas Gerais - FAPEMIG (APQ-02360-18) and (APQ-00777-19) for their support.

## Author Contributions

Roberta Prado was responsible for conceptualization, data curation, formal analysis, investigation, methodology, project administration, writing the original draft; Addila Salgado and Joyce Rodrigues for

investigation and methodology; Cristiane A. Scaldaferrri and Fabiana P. Sousa for data curation, formal analysis and writing the original draft; Vanya M. D. Pasa for conceptualization, data curation formal analysis, funding acquisition, investigation methodology, project administration and writing the original draft; Vera R. L. Constantino for funding acquisition and investigation methodology; Frederico Pinto for project administration, writing and review the original draft; Jairo Tronto for conceptualization, formal analysis, funding acquisition, investigation, methodology, project administration, writing, and review the original draft.

## References

- Kouzu, M.; Fujimori, A.; Suzuki, T.; Koshi, K.; Moriyasu, H.; *Fuel Process. Technol.* **2017**, *165*, 94. [Crossref]
- Galadima, A.; Muraza, O.; *J. Cleaner Prod.* **2020**, *263*, 121358. [Crossref]
- Avhad, M. R.; Marchetti, J. M.; *Renewable Sustainable Energy Rev.* **2015**, *50*, 696. [Crossref]
- Sipos, P.; Pálínkó, I.; *Catal. Today* **2018**, *306*, 32. [Crossref]
- Centi, G.; Perathoner, S.; *Microporous Mesoporous Mater.* **2008**, *107*, 3. [Crossref]
- Dahdah, E.; Estephane, J.; Haydar, R.; Youssef, Y.; El Khoury, B.; Gennequin, C.; Aboukaïs, A.; Abi-Aad, E.; Aouad, S.; *Renewable Energy* **2020**, *146*, 1242. [Crossref]
- Seffati, K.; Esmaeili, H.; Honarvar, B.; Esfandiari, N.; *Renewable Energy* **2020**, *147*, 25. [Crossref]
- Granados-Reyes, J.; Salagre, P.; Cesteros, Y.; *Appl. Clay Sci.* **2016**, *132-133*, 216. [Crossref]
- Creasey, J. J.; Chieragato, A.; Manayil, J. C.; Parlett, C. M. A.; Wilson, K.; Lee, A. F.; *Catal. Sci. Technol.* **2014**, *4*, 861. [Crossref]
- Mora, M.; López, M. I.; Jiménez-Sanchidrián, C.; Ruiz, J. R.; *Catal. Lett.* **2010**, *136*, 192. [Crossref]
- Sánchez-Cantú, M.; Camargo-Martínez, S.; Pérez-Díaz, L. M.; Hernández-Torres, M. E.; Rubio-Rosas, E.; Valente, J. S.; *Appl. Clay Sci.* **2015**, *114*, 509. [Crossref]
- Rousselot, I.; Taviot-Guého, C.; Leroux, F.; Léone, P.; Palvadeau, P.; Besse, J.-P.; *J. Solid State Chem.* **2002**, *167*, 137. [Crossref]
- Díez, V.; Apesteguía, C. R.; Di Cosimo, J.; *J. Catal.* **2003**, *215*, 220. [Crossref]
- Vieille, L.; Rousselot, I.; Leroux, F.; Besse, J.; Taviot-Guého, C.; *Chem. Mater.* **2003**, *15*, 4361. [Crossref]
- Newman, S. P.; Jones, W.; *New J. Chem.* **1998**, *22*, 105. [Crossref]
- Crepaldi, E. L.; Valim, J. B.; *Quim. Nova* **1998**, *21*, 300. [Crossref]
- Prado, R. G.; Almeida, G. D.; de Oliveira, A. R.; de Souza, P. M. T. G.; Cardoso, C. C.; Constantino, V. R.-L.; Pinto, F. G.; Tronto, J.; Pasa, V. M. D.; *Energy Fuels* **2016**, *30*, 6662. [Crossref]
- Rahman, A.; Pullabhotla, R. V. S.; *Bull. Chem. React. Eng. Catal.* **2022**, *17*, 163. [Crossref]
- López-Salinas, E.; Serrano, M. E. L.; Jácome, M. A. C.; Secora, I. S.; *J. Porous Mater.* **1996**, *2*, 291. [Crossref]
- EN 14103:2011: *Fat and Oil Derivatives-Fatty Acid Methyl Esters (FAME) - Determination of Ester and Linolenic Acid Methyl Ester Contents*; European Committee for Standardization, Brussels, 2011. [Link]
- Bejan, C. C. C.; Celante, V. G.; Celante, V. R.; de Castro, E. V. R.; Pasa, V. M. D.; *Energy Fuels* **2014**, *28*, 5128. [Crossref]
- de Roy, A.; Forano, C.; El Malki, K.; Besse, J.-P. In *Expanded Clays and Other Microporous Solids*; Ocelli, M. L.; Robson, H. E., eds.; Springer US: Boston, MA, 1992, p. 108-169.
- Crepaldi, E. L.; Pavan, P. C.; Valim, J. B.; *Chem. Commun.* **1999**, 155. [Crossref]
- Sánchez-Cantú, M.; Barcelos-Santiago, C.; Gomez, C. M.; Ramos-Ramírez, E.; Ruiz Peralta, M. D. L.; Tepale, N.; González-Coronel, V. J.; Mantilla, A.; Tzompantzi, F.; *Int. J. Photoenergy* **2016**, *2016*, ID 5256941. [Crossref]
- Campos-Molina, M. J.; Santamaría-González, J.; Mérida-Robles, J.; Moreno-Tost, R.; Albuquerque, M. C. G.; Bruque-Gámez, S.; Rodríguez-Castellón, E.; Jiménez-López, A.; Maireles-Torres, P.; *Energy Fuels* **2010**, *24*, 979. [Crossref]
- Kuwahara, Y.; Tsuji, K.; Ohmichi, T.; Kamegawa, T.; Mori, K.; Yamashita, H.; *Catal. Sci. Technol.* **2012**, *2*, 1842. [Crossref]
- Zheng, L.; Xia, S.; Lu, X.; Hou, Z.; *Chin. J. Catal.* **2015**, *36*, 1759. [Crossref]
- Knothe, G.; *J. Am. Oil Chem. Soc.* **2000**, *77*, 489. [Crossref]
- Tariq, M.; Ali, S.; Ahmad, F.; Ahmad, M.; Zafar, M.; Khalid, N.; Khan, M. A.; *Fuel Process. Technol.* **2011**, *92*, 336. [Crossref]
- Sankaranarayanan, S.; Antonyraj, C. A.; Kannan, S.; *Bioresour. Technol.* **2012**, *109*, 57. [Crossref]
- Cavani, F.; Trifirò, F.; Vaccari, A.; *Catal. Today* **1991**, *11*, 173. [Crossref]
- Yanishevskii, V. M.; *J. Appl. Spectrosc.* **1992**, *55*, 1224. [Crossref]
- Shuzhi, L.; Bangwei, Z.; Xiaolin, S.; Yifang, O.; Haowen, X.; Zhongyu, X.; *J. Mater. Process. Technol.* **1999**, *89-90*, 405. [https://doi.org/10.1016/S0924-0136(99)00048-5]
- Fleet, M. E.; *Biomaterials* **2009**, *30*, 1473. [Crossref]
- Mahjoubi, F. Z.; Khalidi, A.; Abdennouri, M.; Barka, N.; *J. Taibah Univ. Sci.* **2017**, *11*, 90. [Crossref]
- Constantino, V. R. L.; Pinnavaia, T. J.; *Inorg. Chem.* **1995**, *34*, 883. [Crossref]
- Granados, M. L.; Poves, M. D. Z.; Alonso, D. M.; Mariscal, R.; Galisteo, F. C.; Moreno-Tost, R.; Santamaría, J.; Fierro, J. L. G.; *Appl. Catal., B* **2007**, *73*, 317. [Crossref]
- Kouzu, M.; Hidaka, J.-S.; *Fuel* **2012**, *93*, 1. [Crossref]
- Kouzu, M.; Kasuno, T.; Tajika, M.; Sugimoto, Y.; Yamanaka, S.; Hidaka, J.; *Fuel* **2008**, *87*, 2798. [Crossref]

40. Climent, M. J.; Corma, A.; de Frutos, P.; Iborra, S.; Noy, M.; Velly, A.; Concepción, P.; *J. Catal.* **2010**, *269*, 140. [Crossref]
41. Muráth, S.; Varga, T.; Kukovecz, Á.; Kónya, Z.; Sipos, P.; Pálinkó, I.; Varga, G.; *Mater. Today Chem.* **2022**, *23*, 100682. [Crossref]
42. Zanjani, N. G.; Kamran-Pirzaman, A.; Khalajzadeh, M.; *Clean Technol. Environ. Policy* **2020**, *22*, 1173. [Crossref]
43. Fan, G.; Li, F.; Evans, D. G.; Duan, X.; *Chem. Soc. Rev.* **2014**, *43*, 7040. [Crossref]
44. Lee, H. V.; Taufiq-Yap, Y. H.; Hussein, M. Z.; Yunus, R.; *Energy* **2013**, *49*, 12. [Crossref]
45. Lee, H.; Juan, J.; Binti Abdullah, N.; Nizah, M. F. R.; Taufiq-Yap, Y.; *Chem. Cent. J.* **2014**, *8*, 30. [Crossref]

*Submitted: January 26, 2022*  
*Published online: June 1, 2022*

